Radar-lidar ratio for ice crystals of cirrus clouds

ZHENZHU WANG,[1] [iD] VICTOR SHISHKO,[2] NATALIA KUSTOVA,[2] ALEXANDER KONOSHONKIN,[2,3] DMITRY TIMOFEEV,[2] CHENBO XIE,[1] DONG LIU,[1] AND ANATOLI BOROVOI[2,*] [iD]

[1]*Key Laboratory of Atmospheric Optics, Anhui Institute of Optics and Fine Mechanics, Chinese Academy of Sciences, Hefei 230031, China*
[2]*V. E. Zuev Institute of Atmospheric Optics SB RAS, Academician Zuev Sq. 1, 634055 Tomsk, Russia*
[3]*National Research Tomsk State University, Lenina str. 36, 634050 Tomsk, Russia*
[*]*borovoi@iao.ru*

Abstract: Simultaneous measurement of lidar and radar signals returned from the same cirrus clouds is a prospective method for retrieving the cloud microphysics, i.e. size and shape of the ice crystals constituting the clouds. In this study, the ratio of the backscattered signals of lidar and radar called the radar-lidar ratio has been calculated for the first time for typical shapes of ice crystals and wide distribution of the crystals over their sizes. It is shown that it is the lidar-radar ratio that is most sensitive to crystal sizes while the lidar depolarization ratio is most sensitive to crystal shapes.

1.   Introduction

Cirrus clouds consisting mainly of ice crystals are important components of the atmosphere which essentially modulate the radiative budget of the Earth. Until now, the microphysical properties (i.e., size and shape) of the ice crystals as well as their number density are poorly known because of their great variability in time and space and difficulties of field measurements. These properties are strongly needed for incorporating in up-to-date models of climate [1]. At present, cirrus clouds are widely studied by various ground-based, airborne and spaceborne instruments. Among such instruments, lidars and radars are promising devices providing active remote sensing of the clouds. While earlier works [2–5] considered ground-based instruments, at present the clouds are studying intensively by the space-borne lidar onboard the CALIPSO satellite [6] and by the radar onboard the CloudSat satellite [7]. In the nearest future, lidar and radar will operate together from the EarthCARE satellite [8].

The common values measured by lidars in cirrus are the backscattering coefficient β, extinction coefficient α, and the linear depolarization ratio δ^l. Analogously, radars measure the reflectivity η (or effective reflectivity factor Z_e) and the depolarization ratio δ^r. If lidar or radar is used alone, the measurable quantities give little information on the clouds. To decrease uncertainties in the retrieval procedures, the measured quantities are usually supplemented with the data obtained independently by other instruments like, for example, radiometers (e.g., [9–14]).

It is worthwhile to note that the ice water content (IWC) was often the main object for retrieving. In particular, both the radar reflectivity factor and lidar extinction coefficients were linked with IWC by some empirically obtained power laws (e.g., [3,15–17]). In these power laws, there are different powers of the number density of the crystals in opposite sides of the equation that is difficult for interpretation.

On the contrary, a combined use of lidar and radar sounding simultaneously just the same volume of a cirrus cloud is a promising method for retrieving both the number density and microphysical properties of the ice crystals (e.g., [2,4]). Here the number density of ice crystals and their microphysical properties are the same during measurements. Consequently, the ratio of the backscattered signals of radar and lidar is independent of the particle number density and

this ratio characterizes only the microphysical properties. Then, at the given microphysics, the number density of crystals can be retrieved from one of the measurable quantities: the lidar backscattering/extinction coefficients or the radar reflectivity factor.

The first work combining lidar and radar measurements in cirrus was reported by Intrieri et al. [2] long ago in 1993. These authors managed to retrieve the vertical profiles of the effective crystal size from such measurements. Then Okamoto et al. [4] proposed an algorithm for retrieving both IWC and effective particle size from the data obtained by space-borne lidar-radar measurements. Later other algorithms combining simultaneous measurements from space-borne radiometers, radars and lidars were developed and explored (e.g., [9–14]).

In the papers where both lidar and radar were used, the microphysical properties of ice crystals were inferred from the ratio called here the radar-lidar ratio

$$\chi = \frac{\beta^r}{\beta^l} = \frac{c\sigma^r}{c\sigma^l} = \frac{\sigma^r}{\sigma^l}. \tag{1}$$

In Eq. (1), it is assumed that the crystals are randomly oriented and a receiver of the backscattered signals measures only intensity but not polarization. Here β is the backscattering coefficient, the upper indexes r, l refer to radar or lidar measurements, c is the number density of crystals, and σ is the differential scattering cross section of single crystal in the backward direction. The value σ includes the averaging over a statistical ensemble of crystals presented in a cloud.

However, there is a considerable difficulty of this method. Namely, the radar-lidar ratio χ has not been calculated reliably yet. Indeed, in the pioneer work by Intrieri at al. [2] the ice crystal shapes were assumed as spheres that are far from reality. In this case, the microwave and light backscatter by a crystal was calculated using the well-known Mie theory. Then more realistic nonspherical shapes of ice crystals were suggested and explored [9–14]. For the nonspherical particles, the radar backscattering cross section for one crystal can be easy calculated [18] as a numerical solution to the Maxwell equations by means of the methods like the discrete dipole approximation [19], T-matrix method [20], finite-difference time-domain method, and so on. Unfortunately, these methods are not effective for light backscatter because the crystal sizes are much larger than a lidar wavelength. For calculation of the lidar backscatter, these methods need extremely large computer resources. Also, the common geometrical-optics approximation is not reliable since it ignores the interference and diffraction phenomena that are essential at the backward scattering direction.

It is worthwhile to mention that a comprehensive data library of the light scattering matrixes for ice crystals of cirrus clouds has been recently published [21]. In this work [21], the calculations had been performed mainly with the improved geometric-optics method (IGOM). However, the further work [22] showed that the IGOM was not applicable to the backward scattering direction which was of main importance for lidar studies. As a result, only the physical-optics approximation developed recently [23–32] proves to be effective for solving the problem of light backscatter by ice crystals of cirrus clouds.

The purpose of this paper is to calculate and to place into the public domain the radar-lidar ratio explicitly for the first time at a reasonable model for size and shapes of cirrus ice crystals using the physical-optics approximation [24,26,29–32]. We show that the radar-lidar ratio is a prospective microphysical characteristic of cirrus clouds that is highly informative for retrieving crystal sizes at different crystal shapes.

2. Mueller matrix for randomly oriented particles

If polarization properties of the scattered waves are considered, the waves are characterized by both intensities and polarization states. In general, these values are described by the 4×4 scattering (Mueller) matrix **M** (e.g., [20]). In the beginning, we restrict ourselves by the simplest case of randomly oriented ice crystals. In this case, the Mueller matrix in the backward scattering

direction becomes the diagonal one [20]. Moreover, this diagonal matrix is determined by only two elements M_{11} and M_{22}. Note that, strictly speaking, the element $M_{14} = M_{41}$ is also not zero but it is usually negligible.

This is the first element M_{11} that is equal to the backscattering cross section used in Eq. (1)

$$M_{11}^{r,l} = \sigma^{r,l}. \tag{2}$$

The second element M_{22} of the Mueller matrix normalized as $\gamma^{r,l} = M_{22}^{r,l}/M_{11}^{r,l}$ determines the polarization states of the backscattered radiation. In particular, the conventional linear depolarization ratio δ for both radars and lidars is expressed as

$$\delta^{r,l} = \frac{\sigma_{\perp}^{r,l}}{\sigma_{||}^{r,l}} = \frac{1 - \gamma^{r,l}}{1 + \gamma^{r,l}}, \tag{3}$$

where the lower indexes ⊥ and || correspond to the perpendicular and parallel components of the backscattered radiation relative to incident linearly polarized wave. Any other measurements concerning polarization of the backscattered signals for randomly oriented crystals are readily expressed through the quantities $\sigma^{r,l}$ and $\delta^{r,l}$.

If nonspherical particles are not randomly oriented but have some preferential orientation and the radar-lidar is pointed at arbitrary direction, Eq. (3) becomes complicated. This equation is discussed elsewhere [33].

3. Radar-lidar ratio for randomly oriented ice crystals of cirrus clouds

Shapes of ice crystals naturally occurring in cirrus clouds are strongly various (e.g., see Refs. in [34]). On the one hand, the shapes can be pristine where the crystals of simple shapes are formed according to the crystallographic laws. These pristine shapes are the solid hexagonal ice columns and plates, bullet-rosettes, droxtals, etc. On the other hand, there are crystals of complex shapes as well. They include aggregates consisting of the pristine elements, crystals of irregular shapes, deformed pristine crystals, and so on. It is important that sizes of the ice crystals range from 10 μm up to 2000–4000 μm, i.e. they essentially exceed a lidar wavelength. As for radars, their wavelengths are much larger than crystal sizes.

In this paper, we calculate the radar-lidar ratio for the ice crystal shapes 1–5 of Fig. 1. Here the lidar backscattering cross sections σ^l have been calculated with the physical-optics approximation [26,29–32] while the radar counterparts σ^r are obtained from the discrete dipole approximation [19]. Note that it is the Mueller matrix that is the output of the both codes.
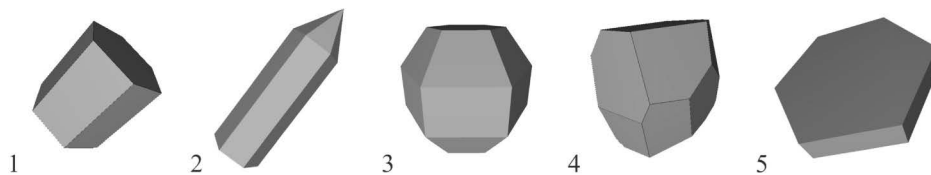

Fig. 1. Shapes of ice crystals used in calculations: 1 – hexagonal column, 2 – bullet; 3 – droxtal, 4 – irregular polyhedron, 5 – hexagonal plate.

Size of the nonspherical crystals is conventionally defined either by the equivalent radius R_{eq} or by the maximum dimension D_{max}. Here R_{eq} means radius of the sphere with the same volume while the maximum dimension D_{max} is equal to the maximum distance between two points on a particle surface. The additional geometrical parameters of the hexagonal ice plates, columns, bullets, and droxtals are taken the same as in Table 1 of [30]. The irregular polyhedron of Fig. 1 is chosen as particle 3 in Fig. 1 of [31]. A part of the numerical data was taken from our data

bank [32] and the deficient data have been calculated separately. The backscatter by an ice sphere with the refractive index of 1.3116 has been calculated by numerical summation of the Mie series. Though the sum of the Mie series is a quickly oscillation function, these oscillations have been smoothed with a procedure of moving average [35]. Note that the refractive indexes of the ice crystals were chosen as $1.7861 + 0.0011i$ and $1.7864 + 0.0032i$ for the frequencies of 35 GHz and 94 GHz, respectively.

Figure 2 shows the radar-lidar ratios calculated for the crystal shapes of Fig. 1 as functions of R_{eq} and $D_{\max}$. The main feature of Fig. 2 is that the curves $\chi(R_{eq})$ and $\chi(D_{\max})$ strongly depend on crystal size. On the contrary, their variations with crystal shapes are rather weak. Consequently, these results prove that it is the lidar-radar ratio that is effective for retrieving the crystal sizes.
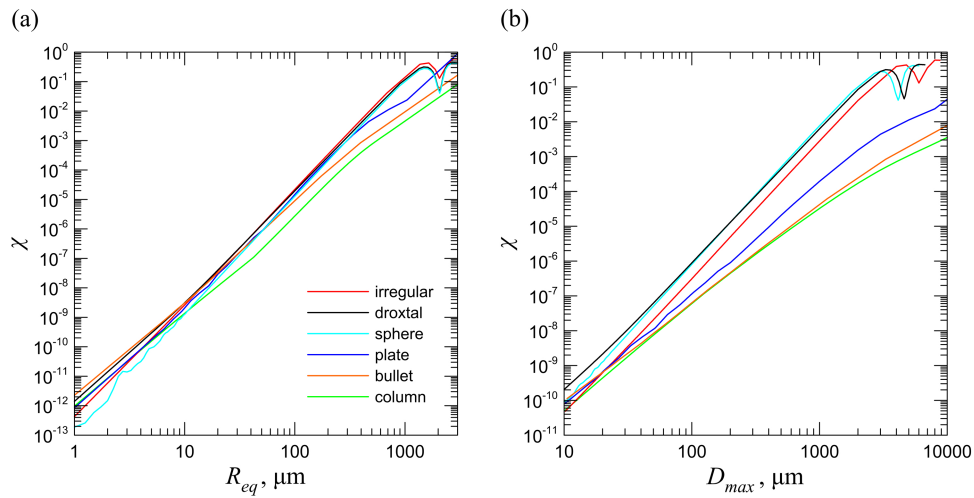
(a)   (b)

Fig. 2. Lidar-radar ratio for various crystal shapes versus: a) the equivalent radius and b) the maximum dimension. Lidar wavelength is 0.532 μm and radar frequency is 35 GHz.

In Fig. 2(b), we see that a set of the curves $\chi(D_{\max})$ is not as compact as in Fig. 2(a). It demonstrates that the size definition through R_{eq} is preferable if anybody uses the radar-lidar ratio for a size retrieving procedure. Therefore, onwards we will use the definition of crystal size through the equivalent radius.

In reality, size of ice crystals in cirrus clouds is not constant; the crystals are widely distributed over their sizes. Let us estimate impact of size distributions on the radar-lidar ratios. For the estimation, we assume the gamma-distribution in its simplest case

$$p(R_{eq}) = R_{eq}e^{-R_{eq}/R_{\mathrm{mod}}} \Big/ \int_{1\,\mu m}^{3000\,\mu m} R_{eq}e^{-R_{eq}/R_{\mathrm{mod}}}\,dR_{eq}. \qquad (4)$$

Applicability of this equation to ice crystals of cirrus clouds is discussed, for example, in [36]. This distribution is characterized by the modal size R_{mod}. The modal size has a simple physical meaning: this is the point $R_{eq} = R_{\mathrm{mod}}$ where the distribution is maximal.

Taking into account the wide distribution of ice crystals over their sizes, it is only the modal size R_{mod} that should be retrieved from any measurable data. Therefore the radar-lidar ratio for the statistical ensembles of ice crystals of the same shapes but distributed over their sizes has been calculated and presented in Fig. 3.
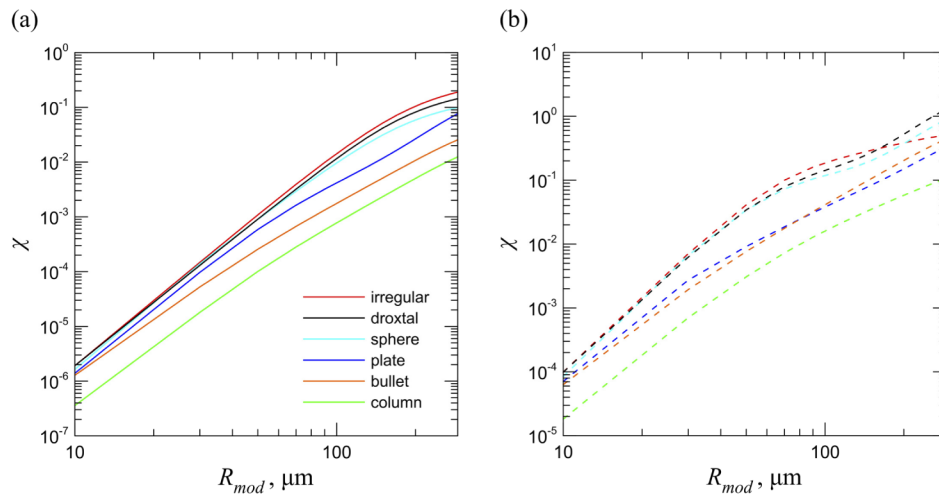
(a)   (b)

Fig. 3. Lidar-radar ratio for the statistical ensembles of ice crystals with the same shapes but distributed over size according to Eq. (4) versus the modal size of the distribution (radar frequencies are 35 GHz (a) and 94 GHz (b)).

Figure 3 shows that if a radar-lidar ratio χ is found experimentally for a cloud with unknown crystal shapes, this quantity χ allows us to find a rather narrow interval for possible modal sizes in this cloud. The physical interpretation of the data presented in Figs. 2 and 3 is discussed in details in Sec. 5.

4. Radar-lidar ratio for clouds of quasi-horizontally oriented hexagonal plates

If lidars sounding cirrus clouds are pointed vertically, the so-called effect of specular reflection is often observed [37,38]. This effect is caused by plate-like crystals with sizes much larger than wavelength which are often oriented quasi-horizontally in the atmosphere [39]. Tilt of the plate-like crystals from horizontal will be denoted by the zenith angle β where the case $\beta = 0°$ corresponds to the horizontal orientation. It is common to assume that the tilts are distributed normally [38,40]

$$p(\beta) = e^{-\beta^2/2\beta_{eff}^2} \Big/ \int\limits_0^{\pi/2} e^{-\beta^2/2\beta_{eff}^2} \sin\beta d\beta, \tag{5}$$

where β_{eff} determines width of the distribution.

The specular reflection effect depends on proportion of the horizontally oriented plate-like crystals in a cloud and their distributions over tilts. Both the proportion of the plate-like crystals and their orientation distributions are strongly variable in the atmosphere. At present, these characteristics are poorly known [38]. Therefore, in this paper, we present only the data that can indicate tendency in changing the radar-lidar ratio when the horizontally oriented plate-like crystals appear in cirrus clouds. More comprehensive study is a subject of further work.

Figure 4 presents the radar-lidar ratio calculated for an ensemble of hexagonal plates distributed over size and tilts according to Eqs. (4) and (5). Figure 4(a) reveals the following important regularity. We see that if lidar is directed vertically and the crystals are oriented horizontally, the radar-lidar ratio is sharply lowered by a factor of 5-9 orders as compared with the case of the quasi-random orientation $\beta_{eff} = 90°$. This result is easy explained by the sharp increase of the lidar backscatter at the normal incidence of light on the horizontally oriented plates. However, if

the plate is tilted, the backscattered light is formed by the Fraunhofer diffraction pattern [40] that is a quickly decreasing value with the tilt angle β. As a result, the light backscatter quickly decreases with the tilt width β_{eff} of Eq. (5). In its turn, the radar backscatter is not so sensitive to the crystal tilts as the lidar counterpart. These two facts lead in Fig. 4(a) to the quick growth of the radar-lidar ratio up to the values shown in Fig. 3(a) for the randomly oriented crystals of the other shapes. Thus, we conclude that appearance of the quasi-horizontally oriented crystals in a cirrus cloud should decrease the radar-lidar ratio.
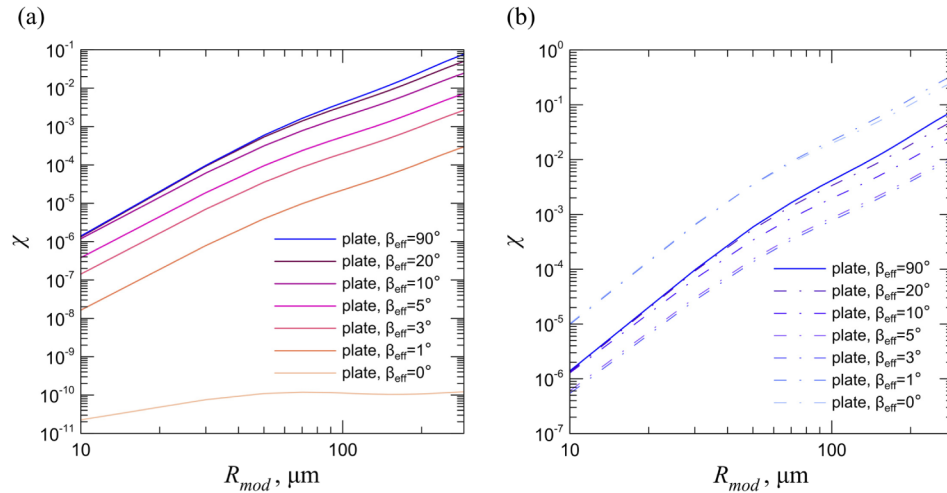
(a) (b)

Fig. 4. Lidar-radar ratio for hexagonal ice plates distributed over size and tilts according to Eqs. (4) and (5), respectively, for the vertically oriented (a) and tilted at 5° (b) radar-lidar system. The radar frequency is 35 GHz.

Sometimes the lidar-radar systems are directed not vertically but they are tilted relative to vertical at the angle T. In this case, the monotonic growth of the radar-lidar ratio with the tilt distribution width β_{eff} is violated. Indeed, the lidar backscatter initially increases until to the value of $\beta_{eff} \approx T$ and then the backscatter decreases according to the Fraunhofer diffraction. Consequently, the function $\chi(\beta_{eff})$ is maximal at $\beta_{eff} \approx T$ that is demonstrated in Fig. 4(b). Note that the lidar tilt of 5° in Fig. 4(b) is chosen only for illustration though the lidar CALIPSO is operating at the tilt of 3°.

5. Depolarization ratios of lidars and radars

In the previous sections, we considered the radar-lidar ratio and demonstrated that this ratio is informative concerning crystal sizes. The next important microphysical property of cirrus clouds is shape of the crystals constituting the clouds. While the radar-lidar ratio is weakly sensitive to the crystal shapes, the common depolarization ratio should be a more sensitive quantity. Theoretically, the linear depolarization ratio for the randomly oriented crystals is obtained from Eq. (3) using the elements of the Mueller matrix M_{11} and M_{22}.

Figure 5(a) shows the lidar depolarization ratio obtained for randomly oriented crystals of the shapes 1–4 of Fig. 1. Here the discrete values denoted by dots have been obtained from magnitudes of the Mueller matrix presented in our data bank [32]. The solid lines are calculated according to the power laws obtained for the Mueller matrix earlier [30]. The good coincidence of the dots and curves supports our previous results. Note that the fracture of the curve for the hexagonal column at about 40 µm is caused by the corresponding fracture of the aspect ratio according to the common shape model for the ice hexagonal columns [41].
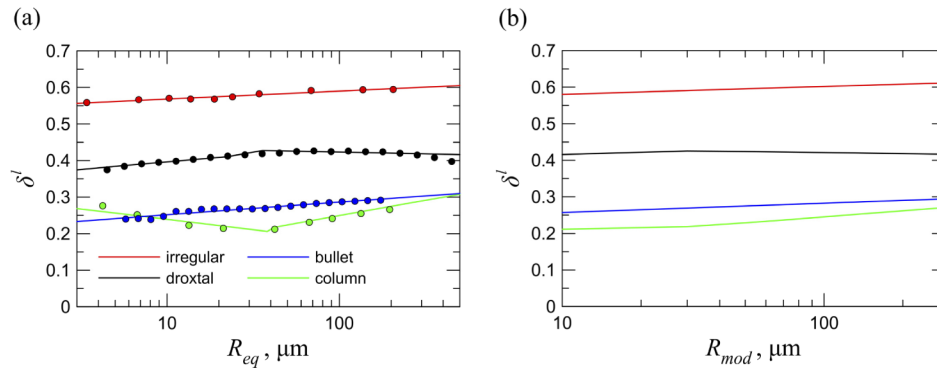
(a)   (b)

Fig. 5. Lidar depolarization ratio for various crystal shapes versus: a) equivalent radius; b) modal size. Lidar wavelength is 0.532 µm.

Figure 4(a) reveals three remarkable properties. First, the depolarization ratios weakly depend on crystal size. Practically, we can assume them as constants. Second, these quasi-constants essentially depend on crystal shape; the quantity δ^l ranges from about 20% for the column to about 60% for the irregular polyhedron.

Third, the curves $\delta^l(R_{eq})$ line up in the same order as it took place for the radar-lidar ratio in Figs. 2 and 3. Namely, the hexagonal column and irregular polyhedron produce the minimum and maximum limiting curves $\delta^l(R_{eq})$ while the bullet and droxtal give intermediate magnitudes. Analogously to the lidar-radar ratio, we suggest that other shapes or mixtures of shapes should give some intermediate quasi-constant depolarization ratios δ^i as well.

Figure 4(b) shows the depolarization ratios obtained for the statistical ensembles of crystals of the same shape but distributed over their sizes according to Eq. (4). We see that the averaging procedure only refines the three properties of the curves of Fig. 4(a) discussed above. Thus, we conclude that it is the lidar depolarization ratio that should be used for inferring crystal shapes independently of crystal size.

As for the radar depolarization ratio $\delta^r(R_{eq})$, it has been calculated with the discrete-dipole approximation. The results are shown in Fig. 6. Unlike the lidar depolarization ratios, the functions $\delta^r(R_{eq})$ demonstrate complicated dependence on crystal shape and size. Consequently, these functions are not prospective for using them in retrieval procedures. Moreover, their magnitudes are small $\delta^r \leq 4\%$ that is an additional obstacle for using them in a retrieval of the microphysics.
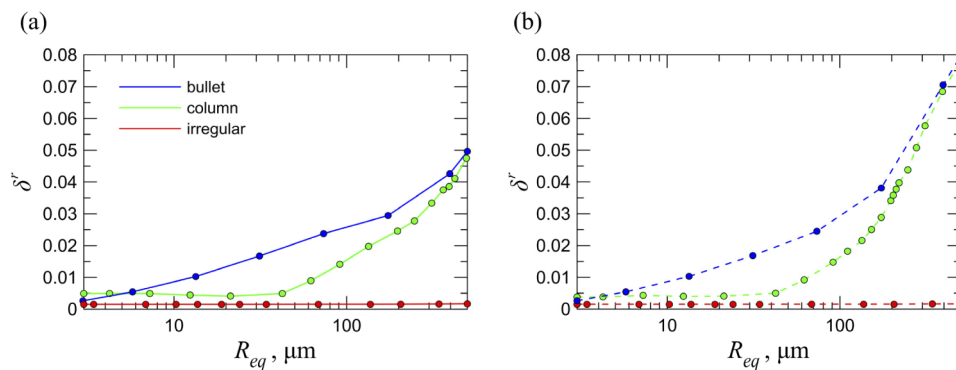
(a)   (b)

Fig. 6. Radar depolarization ratio for different crystal shapes (radar frequencies are 35 GHz (a) and 94 GHz (b)).

In reality, a cirrus cloud is an ensemble of crystals with unknown shapes and sizes. Of course, two measurable quantities χ and δ^l don't determine the statistical ensemble exactly. Nevertheless, a simultaneous use of the two quantities χ and δ^l looks a promising method for inferring the modal size and shape of the crystals from Figs. 3 and 5.

6. Discussion

The numerical data, obtained in this paper for the radar-lidar ratio, can be explained using the physical interpretation developed earlier. Namely, in [26,29] we showed that the lidar backscattering cross section σ^l of ice crystals of cirrus clouds is enhanced by the corner-reflection effect. This effect is produced by the orthogonal facets of the crystals if such facets occurred. These facets operate as 2D corner reflectors at random crystal orientations. This is the additional quantity that appeared in the backscatter because of the facet orthogonality is called the corner-reflection effect. As for the angular distribution of the scattered radiation, these orthogonal facets create a narrow backscattering peak because of the Fraunhofer diffraction of the plane-parallel beams leaving a crystal facet [29].

Coming back to Fig. 2(a), we see that the curves $\chi(R_{eq})$ for different crystal shapes line up according to magnitudes of the corner-reflection effect for these shapes. Indeed, among the shapes 1–4 of Fig. 1, the corner-reflection effect is maximal for the hexagonal column since the orthogonal facets are mostly pronounced in this geometrical shape. Since the lidar backscattering cross section is placed in the denominator of Eq. (1), the hexagonal column gives the minimal radar-lidar ratio $\chi_{col}(R_{eq})$. Then, at the same crystal volumes, the contribution of the orthogonal facets to backscattering for bullets decreases as compared to the case of hexagonal columns. Here the numerator weakly varies for different shapes because of the quasi-Rayleigh scattering of the microwaves. Consequently, we get $\chi_{bul}(R_{eq}) > \chi_{col}(R_{eq})$. The same is true for droxtals, i.e. $\chi_{drox}(R_{eq}) > \chi_{bul}(R_{eq})$. At last, the irregular polyhedron 4 has no orthogonal facets. Here the corner-reflection effect disappears and the function $\chi_{irreg}(R_{eq})$ is maximal. It is interesting that the curve $\chi_{irreg}(R_{eq})$ practically coincides with the curve obtained for the ice sphere. It is important that the same regularities become more visual for the ensembles of crystals characterized by their modal size R_{mod} as shown in Fig. 3.

To support this point of view, we have calculated the radar-lidar ratio for the distorted hexagonal column with the distortion angle ξ that is determined in [29] (see Fig. 7(a)). Here increase of the angle ξ distorting the orthogonality of facets should weaken the corner-reflection effect. We assume that the distortion angle is distributed normally like Eq. (5) with the width ξ_{eff}. Consequently, the radar-lidar ratio increases with the width ξ_{eff} that is demonstrated in Fig. 7.

Let us discuss possibilities to use the data obtained in Fig. 3 for retrieving the microphysics, i.e. size and shape of the ice crystals. If anybody has some model for crystal shapes in a cloud, it is easy to calculate numerically the lidar-radar ratio $\chi(R_{mod})$ for this model. Then, at the experimentally measured value of the lidar-radar ratio, the curve of the figure like Fig. 3 will allow to retrieve the desired modal size. However, in practice, the shape model is not known. In this case, at a given value of the lidar-radar ratio, Fig. 3 provides an interval for the possible magnitudes of the modal size. Here the minimal and maximal values of the modal size correspond to the case of the irregular polyhedron and hexagonal column, respectively.

Basing on the physical interpretation of Fig. 3, we could suggest that the curves $\chi(R_{mod})$ calculated for any crystal shape or any shape mixture should be localized between the limiting curves obtained for the irregular polyhedron and hexagonal column in Fig. 3. Indeed, the orthogonal facets are mostly pronounced for the hexagonal columns as compared with other pristine crystal shapes, while the irregular shape 4 of Fig. 1 provides absence of the corner-reflection effect. So, Fig. 3 could be used in practice for estimating the modal crystal sizes in cirrus clouds independently of their shapes. However, one would take into account that appearance of
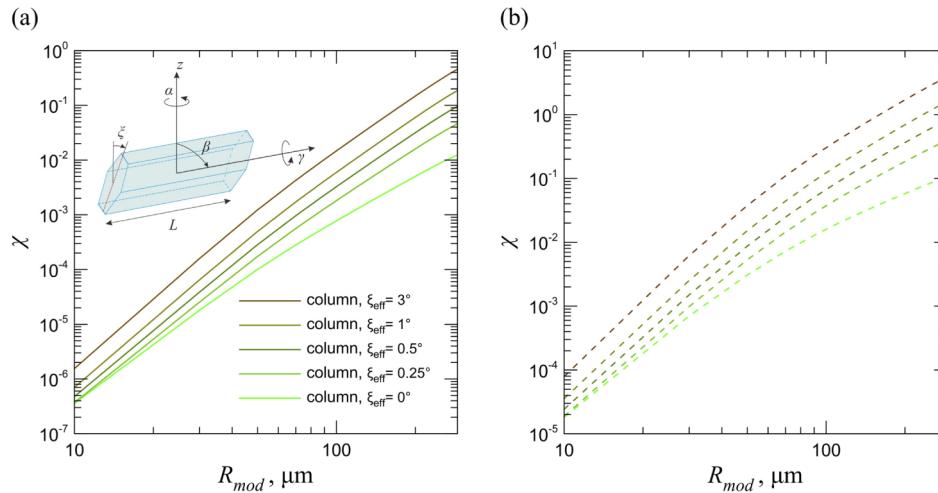
Fig. 7. Lidar-radar ratio for distorted hexagonal columns with the distortion angles ξ distributed normally like Eq. (5) with various widths ξ_{eff} (radar frequencies are 35 GHz (a) and 94 GHz (b)).

plate-like crystals with quasi-horizontal orientations can essentially change magnitudes of the radar-lidar ratio.

7. Conclusions

In conclusion, it is worthwhile to begin with comparison of this paper with a number of papers by other authors [2–5,9–14,42,43] developing algorithms for retrieving microphysical properties of cirrus clouds from the signals obtained with different observation systems (including lidars, radars. radiometers, and other instruments). The aim of this paper is not a development of an algorithm suitable for a given observation system. We would like to refine some general physical regularities. Therefore we assume a lot of assumptions that allow us to discuss the regularities without additional mathematical complications. Thus, we ignore extinction and multiple scattering of radiation which are essential for space-borne observation systems.

In this study, we have explicitly calculated the radar-lidar ratio for the first time for a reasonable model of shapes and sizes of the ice crystals using our code of the physical-optics approximation [32]. As a result, we show that the radar-lidar ratio simply depends on crystal size and this dependence is close to the power law for the backscattering cross section published recently [30]. Also, we obtain that the definition of ice crystal size through the equivalent radius, as compared with the maximum dimension, is preferable for retrieving crystal size (see Fig. 2).

Our treatment of the corner-reflection effect has allowed us to systemize the dependence of the lidar depolarization ratio on crystal shape (see Fig. 5). Note that the experimentally measured lidar depolarization ratio χ is usually equal to about 0.4 in the case of randomly oriented crystals. On the one hand, the case of $\chi \approx 0.4$ in Fig. 5 corresponds to the droxtal shape. On the other hand, it is easy to obtain that the common case of $\chi \approx 0.4$ corresponds also to a mixture of the irregular and regular crystal shapes.

We show that if the radar-lidar ratio χ for a cirrus cloud is found experimentally, Figs. 2 and 3 allow one to infer an interval for possible crystal sizes in the cloud at a given crystal shape. Additionally, if the lidar depolarization ratio δ^l is obtained experimentally for the cloud, too, two quantities χ and δ^l could be a base for creation of algorithms inferring both sizes and shapes of the ice crystals in this cloud.

Disclosures. The authors declare no conflicts of interest.

References

1. D. E. Waliser, J.-L. F. Li, C. P. Woods, R. T. Austin, J. Bacmeister, J. Chern, A. Del Genio, J. H. Jiang, Z. Kuang, H. Meng, P. Minnis, S. Platnick, W. B. Rossow, G. L. Stephens, S. Sun-Mack, W.-K. Tao, A. M. Tompkins, D. G. Vane, C. Walker, and D. Wu, "Cloud ice: A climate model challenge with signs and expectations of progress," J. Geophys. Res. **114**, D00A21 (2009).
2. J. M. Intrieri, G. L. Stephens, W. L. Eberhard, and T. Uttal, "A Method for Determining Cirrus Cloud Particle Sizes Using Lidar and Radar Backscatter Technique," J. Appl. Meteorol. **32**(6), 1074–1082 (1993).
3. Z. Wang and K. Sassen, "Cirrus Cloud Microphysical Property Retrieval Using Lidar and Radar Measurements. Part I: Algorithm Description and Comparison with In Situ Data," J. Appl. Meteorol. **41**(3), 218–229 (2002).
4. H. Okamoto, S. Iwasaki, M. Yasui, H. Horie, H. Kuroiwa, and H. Kumagai, "An algorithm for retrieval of cloud microphysics using 95-GHz cloud radar and lidar," J. Geophys. Res. **108**(D7), 4226 (2003).
5. C. Tinel, J. Testud, J. Pelon, R. J. Hogan, A. Protat, J. Delanoë, and D. Bouniol, "The Retrieval of Ice-Cloud Properties from Cloud Radar and Lidar Synergy," J. Appl. Meteorol. **44**(6), 860–875 (2005).
6. D. M. Winker, M. A. Vaughan, A. Omar, Y. Hu, K. A. Powell, Z. Liu, W. H. Hunt, and S. A. Young, "Overview of the CALIPSO Mission and CALIOP Data Processing Algorithms," J. Atmos. Oceanic Technol. **26**(11), 2310–2323 (2009).
7. G. L. Stephens, D. G. Vane, S. Tanelli, E. Im, S. Durden, M. Rokey, D. Reinke, P. Partain, G. G. Mace, R. Austin, T. L'Ecuyer, J. Haynes, M. Lebsock, K. Suzuki, D. Waliser, D. Wu, J. Kay, A. Gettelman, Z. Wang, and R. Marchand, "CloudSat mission: Performance and early science after the first year of operation," J. Geophys. Res. **113**, D00A18 (2008).
8. A. J. Illingworth, H. W. Barker, A. Beljaars, M. Ceccaldi, H. Chepfer, N. Clerbaux, J. Cole, J. Delanoë, C. Domenech, D. P. Donovan, S. Fukuda, M. Hirakata, R. J. Hogan, A. Huenerbein, P. Kollias, T. Kubota, T. Nakajima, T. Y. Nakajima, T. Nishizawa, Y. Ohno, H. Okamoto, R. Oki, K. Sato, M. Satoh, M. W. Shephard, A. Velázquez-Blázquez, U. Wandinger, T. Wehr, and G.-J. van Zadelhoff, "The EarthCARE Satellite: The Next Step Forward in Global Measurements of Clouds, Aerosols, Precipitation, and Radiation," Bull. Amer. Meteor. Soc. **96**(8), 1311–1332 (2015).
9. D. P. Donovan, A. C. A. P. Van Lammeren, R. Hogan, H. Russchenberg, A. Apituley, P. Francis, J. Testud, J. Pelon, M. Quante, and J. Agnew, "Combined radar and lidar cloud remote sensing: Comparison with IR radiometer and in-situ measurements," Phys. Chem. Earth (B) **25**(10-12), 1049–1055 (2000).
10. J. Delanoë and R. J. Hogan, "Combined CloudSat-CALIPSO-MODIS retrievals of the properties of ice clouds," J. Geophys. Res. **115**, D00H29 (2010).
11. A. Protat, J. Delanoë, E. J. O'Connor, and T. S. L'Ecuyer, "The Evaluation of CloudSat and CALIPSO Ice Microphysical Products Using Ground-Based Cloud Radar and Lidar Observations," J. Atmos. Oceanic Technol. **27**(5), 793–810 (2010).
12. L. A. Borg, R. E. Holz, and D. D. Turner, "Investigating cloud radar sensitivity to optically thin cirrus using collocated Raman lidar observations," Geophys. Res. Lett. **38**(5), 1 (2011).
13. M. Deng, G. G. Mace, Z. Wang, and H. Okamoto, "Tropical Composition, Cloud and Climate Coupling Experiment validation for cirrus cloud profiling retrieval using CloudSat radar and CALIPSO lidar," J. Geophys. Res. **115**, D00J15 (2010).
14. M. Deng, G. G. Mace, Z. Wang, and R. P. Lawson, "Evaluation of Several A-Train Ice Cloud Retrieval Products with In Situ Measurements Collected during the SPARTICUS Campaign," J. Appl. Meteorol. Climatol. **52**(4), 1014–1030 (2013).
15. C.-L. Liu and A. J. Illingworth, "Toward More Accurate Retrievals of Ice Water Content from Radar Measurements of Clouds," J. Appl. Meteorol. **39**(7), 1130–1146 (2000).
16. A. J. Heymsfield, D. Winker, and G.-J. van Zadelhoff, "Extinction-ice water content-effective radius algorithms for CALIPSO," Geophys. Res. Lett. **32**(10), L10807 (2005).
17. M. Avery, D. Winker, A. Heymsfield, M. Vaughan, S. Young, Y. Hu, and C. Trepte, "Cloud ice water content retrieved from the CALIOP space-based lidar," Geophys. Res. Lett. **39**(5), 1 (2012).
18. R. Ekelund and P. Eriksson, "Impact of ice aggregate parameters on microwave and sub-millimetre scattering properties," J. Quant. Spectrosc. Radiat. Transfer **224**, 233–246 (2019).
19. M. A. Yurkin and A. G. Hoekstra, "The discrete-dipole-approximation code ADDA: Capabilities and known limitations," J. Quant. Spectrosc. Radiat. Transfer **112**(13), 2234–2247 (2011).
20. M. I. Mishchenko, J. W. Hovenier, and L. D. Travis, *Light Scattering by Nonspherical Particles* (Academic Press, 2000).

21. P. Yang, L. Bi, B. A. Baum, K.-N. Liou, G. W. Kattawar, M. I. Mishchenko, and B. Cole, "Spectrally Consistent Scattering, Absorption, and Polarization Properties of Atmospheric Ice Crystals at Wavelengths from 0.2 to 100 μm," J. Atmos. Sci. **70**(1), 330–347 (2013).

22. J. Ding, P. Yang, R. E. Holz, S. Platnick, K. G. Meyer, M. A. Vaughan, Y. Hu, and M. D. King, "Ice cloud backscatter study and comparison with CALIPSO and MODIS satellite data," Opt. Express **24**(1), 620–636 (2016).

23. M. Del Guasta, "Simulation of LIDAR returns from pristine and deformed hexagonal ice prisms in cold cirrus by means of "face tracing"," J. Geophys. Res. **106**(D12), 12589–12602 (2001).

24. A. G. Borovoi and I. A. Grishin, "Scattering matrices for large ice crystal particles," J. Opt. Soc. Am. A **20**(11), 2071–2080 (2003).

25. L. Bi, P. Yang, G. W. Kattawar, Y. Hu, and B. A. Baum, "Scattering and absorption of light by ice particles: Solution by a new physical-geometric optics hybrid method," J. Quant. Spectrosc. Radiat. Transfer **112**(9), 1492–1508 (2011).

26. A. Borovoi, A. Konoshonkin, and N. Kustova, "Backscattering by hexagonal ice crystals of cirrus clouds," Opt. Lett. **38**(15), 2881–2884 (2013).

27. C. Zhou and P. Yang, "Backscattering peak of ice cloud particles," Opt. Express **23**(9), 11995–12003 (2015).

28. K. Masuda and H. Ishimoto, "Backscatter ratios for nonspherical ice crystals in cirrus clouds calculated by geometrical-optics-integral-equation method," J. Quant. Spectrosc. Radiat. Transfer **190**, 60–68 (2017).

29. A. Borovoi, N. Kustova, and A. Konoshonkin, "Interference phenomena at backscattering by ice crystals of cirrus clouds," Opt. Express **23**(19), 24557–24571 (2015).

30. A. Konoshonkin, A. Borovoi, N. Kustova, and J. Reichardt, "Power laws for backscattering by ice crystals of cirrus clouds," Opt. Express **25**(19), 22341–22346 (2017).

31. V. Shishko, A. Konoshonkin, N. Kustova, D. Timofeev, and A. Borovoi, "Coherent and incoherent backscattering by a single large particle of irregular shape," Opt. Express **27**(23), 32984–32993 (2019).

32. https://github.com/sasha-tvo/Beam-Splitting. Branch: physical-optics

33. A. G. Borovoi, A. V. Konoshonkin, N. V. Kustova, and I. A. Veselovskii, "Contribution of corner reflections from oriented ice crystals to backscattering and depolarization characteristics for off-zenith lidar profiling," J. Quant. Spectrosc. Radiat. Transfer **212**, 88–96 (2018).

34. A. J. Baran, "A review of the light scattering properties of cirrus," J. Quant. Spectrosc. Radiat. Transfer **110**(14-16), 1239–1260 (2009).

35. V. A. Shishko, A. V. Konoshonkin, N. V. Kustova, and D. N. Timofeev, "Light scattering by spherical particles for data interpretation of mobile lidars," Opt. Eng. **59**(08), 083103 (2020).

36. K. Sato and H. Okamoto, "Characterization of Ze and LDR of nonspherical and inhomogeneous ice particles for 95-GHz cloud radar: Its implication to microphysical retrievals," J. Geophys. Res. **111**(D22), D22213 (2006).

37. C. M. R. Platt, N. L. Abshire, and G. T. McNice, "Some Microphysical Properties of an Ice Cloud from Lidar Observation of Horizontally Oriented Crystals," J. Appl. Meteorol. **17**(8), 1220–1224 (1978).

38. V. Noel and K. Sassen, "Study of Planar Ice Crystal Orientations in Ice Clouds from Scanning Polarization Lidar Observations," J. Appl. Meteorol. **44**(5), 653–664 (2005).

39. J. D. Klett, "Orientation Model for Particles in Turbulence," J. Atmos. Sci. **52**(12), 2276–2285 (1995).

40. A. Borovoi, A. Konoshonkin, N. Kustova, and H. Okamoto, "Backscattering Mueller matrix for quasi-horizontally oriented ice plates of cirrus clouds: application to CALIPSO signals," Opt. Express **20**(27), 28222–28233 (2012).

41. D. L. Mitchell and W. P. Arnott, "A Model Predicting the Evolution of Ice Particle Size Spectra and Radiative Properties of Cirrus Clouds. Part II: Dependence of Absorption and Extinction on Ice Crystal Morphology," J. Atmos. Sci. **51**(6), 817–832 (1994).

42. M. Ceccaldi, J. Delanoë, R. J. Hogan, N. L. Pounder, A. Protat, and J. Pelon, "From CloudSat-CALIPSO to EarthCare: Evolution of the DARDAR cloud classification and its comparison to airborne radar-lidar observations," J. Geophys.Res. Atmos. **118**(14), 7962–7981 (2013)..

43. Q. Cazenave, M. Ceccaldi, J. Delanoë, J. Pelon, S. Groß, and A. Heymsfield, "Evolution of DARDAR-CLOUD ice cloud retrievals: new parameters and impacts on the retrieved microphysical properties," Atmos. Meas. Tech. **12**(5), 2819–2835 (2019)..